Available online at www.sciencedirect.com
ScienceDirect
Catalysis Today 130 (2008) 337–344
CATALYSIS TODAY
www.elsevier.com/locate/cattod

Synthesis, characterization and evaluation of NiMo/SiO_2–Al_2O_3 catalysts prepared by the pH-swing method

César Fernández-Vargas [a], Jorge Ramírez [a,*], Aída Gutiérrez-Alejandre [a], Felipe Sánchez-Minero [b], Rogelio Cuevas-García [a], Pablo Torres-Mancera [a]

[a] *UNICAT, Departamento de Ingeniería Química, Facultad de Química, UNAM, Cd. Universitaria, México 04510, D.F., Mexico*
[b] *DIQP, ESIQIE-Instituto Politécnico Nacional, Zacatenco, México 07738, D.F., Mexico*

Abstract

NiMo/(*X*)SiO_2–Al_2O_3 catalysts were synthesized with various SiO_2 contents (*X* = 0, 10, 25 and 50 wt%) using the pH-swing method. In order to find the optimum SiO_2 content, the catalysts were evaluated in the hydrodesulfurization of 4,6-DMDBT, hydrogenation of naphthalene and hydrodenitrogenation of carbazole. Kinetic parameters of Langmuir–Hinshelwood type equations for all the reaction systems were estimated. FTIR analysis of CO adsorption for the sulfided catalysts shows that the amount of coordinatively unsaturated Mo sites promoted by nickel (CUS-NiMoS) follows the order NiMo/10ASA > NiMo/25ASA > NiMo/0ASA. This tendency agrees with the results obtained in catalytic activity.

Keywords: Hydrodesulfurization; 4,6-DMDBT; Naphthalene; Carbazole; Hydrogenation; NiMo/SiO_2–Al_2O_3 catalysts; L–H equations

1. Introduction

Fossil fuels are and will be for many years more the main energy source due to its lower cost and high efficiency in their transformation. However, due to more and more restrictive environmental regulations on sulfur content for transportation fuels, the refining industry needs to improve the performance of the hydrodesulfurization (HDS) catalysts.

To fulfill the environmental regulations existing today, it is necessary to eliminate the most refractory sulfur compounds present in the intermediate distillates. Literature reports [1–6] indicate that the desulfurization of 4,6-dimethyldibenzothiophene (4,6-DMDBT), one of the most refractory molecules to HDS, occurs by several reaction routes like direct desulfurization (DDS), hydrogenation (HYD) and isomerization (ISOM), being hydrogenation the most favored route [7–10]. However, HDS of 4,6-DMDBT may be affected by the presence of aromatic and nitrogen compounds. Recently, it has been established that nitrogen compounds of the carbazole type greatly influence the performance of HDS catalysts [11–14] since this compound presents an adsorption similar to that of substituted dibenzothiophenes.

To diminish the effect caused by the presence of aromatic and nitrogen compounds is necessary to obtain a catalyst that improves the catalytic activity for the transformation of nitrogen and sulfur compounds. It is known that a strong interaction between active phase and support leads to good dispersion but increases the difficulty to achieve full sulfidation of the Mo oxide phase [2]. On the other hand, a weak interaction between the Mo precursor and the support leads to good sulfidation but at the same time to agglomeration and sintering of the active MoS_2 phase. Therefore, tuning the active phase–support interaction is of great importance to achieve proper sulfidation and dispersion of the active phase [15,16]. When silica is incorporated to the alumina support a decrease in the interaction oxide phase–support is observed [17]. The incorporation of silica to the alumina support by pH-swing method previously reported by Denni [18] could be an alternative for obtaining catalysts with low active phase–support interaction and enhanced hydrogenation capabilities. The pH-swing method consists of a series of stages where the support precursor salts of aluminium and silicon are integrated at two different values of pH (acid and basic zone) to obtain a precipitate (hydroxide of aluminium or silicon). In this method,

* Corresponding author.
E-mail address: jrs@servidor.unam.mx (J. Ramírez).

0920-5861/$ – see front matter
doi:10.1016/j.cattod.2007.10.101

the process of dissolution–precipitation induced by the change of pH can help to obtain a support with controlled textural and mechanical properties. For example, Denni [18] proposed the incorporation of the silica using this method to obtain a mesoporous material with high-surface area (up 300 m^2) and pore sizes of 250–500 Å. This method was designed by Ono et al. [19] to prepare an alumina support with better pore distribution. In agreement with previous studies, the pH-swing method is attractive for the preparation of silica–alumina supports since it can modify the pore structure of these materials in the micro- and macro-porosity range. Other advantages of the method are a smaller time of preparation compared with conventional procedures [20], and an increase in the mechanical strength of the material produced [21].

The aim of this work is to find the SiO_2 content that leads to the optimum performance in the HDS and HDN reaction for the $NiMo/SiO_2–Al_2O_3$ catalysts during the hydrodesulfurization of 4,6-dimethyldibenzothiophene, the hydrogenation of naphthalene and the hydrodenitrogenation of carbazol. To this end, $NiMo/SiO_2–Al_2O_3$ catalysts were prepared with various SiO_2 loadings ($X = 0$, 10, 25 and 50 wt%) by the pH-swing method. The catalysts were evaluated in the hydrodesulfurization (HDS) of 4,6-DMDBT, carbazole hydrodenitrogenation (HDN), and naphthalene hydrogenation (HYD). A kinetic equation was fitted to the catalytic activity results allowing the comparison of kinetic parameters to find the optimum SiO_2 content. The catalyst samples were characterized by FTIR-CO adsorption (sulfided catalysts) and the hydroxyl region was observed to characterize the type of OHs present on the support surface. The dispersion of MoS_2 in the sulfided catalysts was analyzed by high-resolution transmission electron microscopy (HRTEM).

2. Experimental

2.1. Catalysts preparation

Supports with different silica loadings were synthesized by the pH-swing method at 353 K following the method reported previously [18,19]. Fig. 1 shows a simplified diagram of pH-swing method.

Two initial solutions: sodium aluminate (basic precursor of aluminum) and sodium orthosilicate (basic precursor of silicon) were maintained in continuous agitation at 353 K and at pH 10. The first pH change to acid conditions was achieved by the addition of a third solution of aluminum sulfate (acid precursor of aluminum), until pH 4 is reached. The return to basic conditions (pH 10) was accomplished with the incorporation of the basic precursors (sodium aluminate). The two former steps

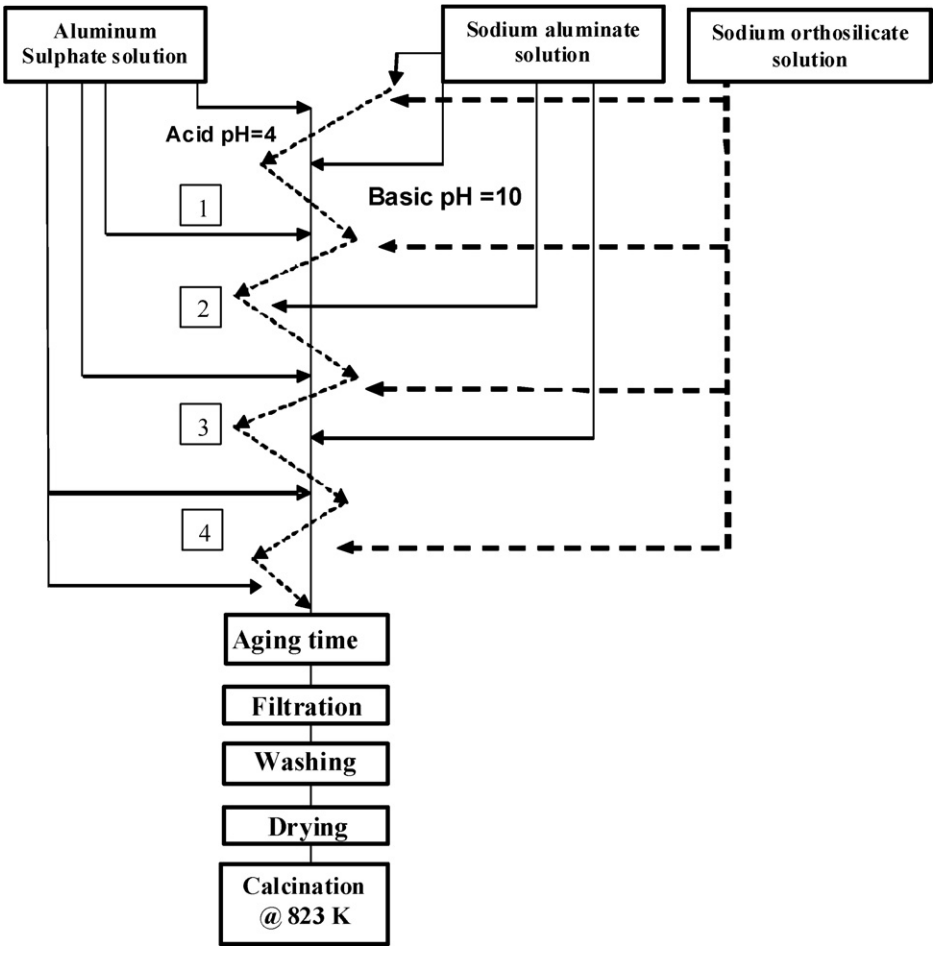

Fig. 1. pH-swing procedure with four changes of pH, from acid to basic zone.

represent an oscillation and it is possible to stay at a fixed pH point an arbitrary residence time. In the present work four oscillations were carried out with residence times in each pH points of 30 min and 24 h at the conclusion of the oscillatory steps. Then, the resulting material was filtered and washed with a solution of ammonium hydroxide to eliminate sodium ions, dried at 393 K and calcined at 823 K. Hereafter supports were labeled as *X*ASA, where $X = 0$, 10, 25 and 50 wt% SiO_2.

The catalysts were impregnated by successive impregnation (pore volume method) of Mo and Ni, respectively. Aqueous solutions of ammonium heptamolybdate and nickel nitrate were used in appropriate amounts of Mo and Ni to obtain a concentration of 2.8 Mo atoms/nm^2 and a ratio of Ni/(Ni + Mo) = 0.3. The support impregnated with ammonium heptamolybdate was dried at 373 K for 24 h and calcined at 773 k for 4 h. Then, nickel was incorporated by impregnation with a solution of nickel nitrate. The catalyst was dried at 373 K for 12 h and calcined at 773 K for 4 h. Here after, the catalysts will be labeled NiMo/*X*ASA, where *X* represents the SiO_2 wt% content on the support.

2.2. Catalytic activity

The catalytic tests were conducted on a batch reactor operating at 1200 psi and 598 K. The catalysts were sulfided "ex situ" in a continuous flow reactor at an atmospheric pressure and 673 K for 4 h using a 15% H_2S/H_2 gas mixture. For the reaction tests, the batch reactor was loaded with 250 mg of sulfided catalyst and 40 ml of the reactive solution. For the reaction tests, *n*-decane was used as solvent. For HDS, a solution of 4,6-DMDBT containing 1000 ppm as sulfur was used. For the HYD test, a solution of 5 wt% naphthalene in decane was employed. And finally, for HDN, a mixture *n*-decane/*m*-xylene (70/30 wt%) was necessary to allow the dissolution of 100 ppm as *N* of carbazole. Analysis of the reaction products was performed with a HP 6890 chromatograph. Additionally, reaction products were identified by GC-mass spectrometry.

2.3. Characterization

Textural properties of catalysts and supports were determined by nitrogen physisorption on a TriStar Micromeritics instrument. Before measurements, the samples were outgassed at 543 K under vacuum during 4 h. The isoelectric point of the supports was measured by electrophoresis using a Z-Meter 3.0+ apparatus. The electrolytic agent was LiCl (0.1N) and the pH was controlled with HCl or LiOH.

FTIR analysis was performed in the 2900–3800 cm^{-1} range, where the observation of the hydroxyl region is possible. A thin wafer of the pure powder was placed into a special IR cell and pretreated under vacuum at 773 K for 1 h. The IR spectra were obtained with a Nicolet Magna 760 FTIR spectrometer using 200 scans and 2 cm^{-1} resolution. CO adsorption on the sulfided catalysts was also followed by FTIR. In this case, sulfidation of the catalysts was performed in situ at 673 K for 4 h in a stream of 20 ml/min of H_2S/H_2 (15%, v/v). The powdered catalysts were pressed into self-supporting wafers (10–14 mg/cm^2) and then sulfided in a high-vacuum glass cell connected to a gas manipulation manifold. After that, the sulfided sample was pretreated by outgassing for 2 h at 723 K. Then small doses of CO at low temperature (100 K) were introduced into the cell until an equilibrium pressure of 1 Torr was reached. After each pulse, the corresponding spectrum was obtained.

For the dispersion analysis, sulfided catalysts were characterized by HRTEM using a JEOL 2010 microscope with a 1.9 Å point-to-point resolution.

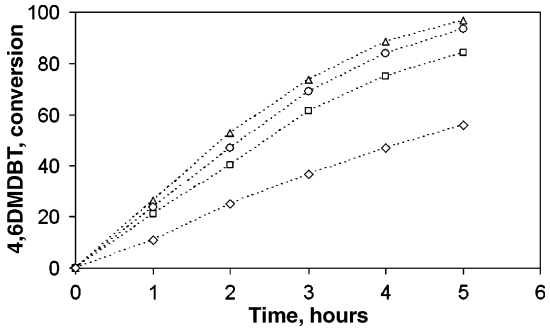

Fig. 2. 4,6-DMDBT conversion for NiMo/0ASA (□), NiMo/10ASA (△), NiMo/25ASA (○) and NiMo/50ASA (◇) at 1200 psi and 598 K.

3. Results and discussion

3.1. Catalytic activity

3.1.1. 4,6-DMDBT hydrodesulfurization

Fig. 2 presents the 4,6-DMDBT HDS conversion for all catalysts. After 5 h reaction time NiMo/10ASA reaches a conversion of nearly 97% compared with 94%, 84% and 56% displayed by NiMo/25ASA, NiMo/0ASA and NiMo/50ASA, respectively. This result shows an increase in the HDS activity when silica is incorporated to the support (10 and 25 wt% SiO_2). However, when the SiO_2 content in the support was 50 wt%, catalytic activity decreased. This catalyst presents the lowest conversion. Therefore, the NiMo/50ASA catalyst was not used in the following tests due its low performance.

3.1.2. Naphthalene hydrogenation

Fig. 3 shows that when the silica loading increases so does the hydrogenation of naphthalene. After 1.25 h reaction time

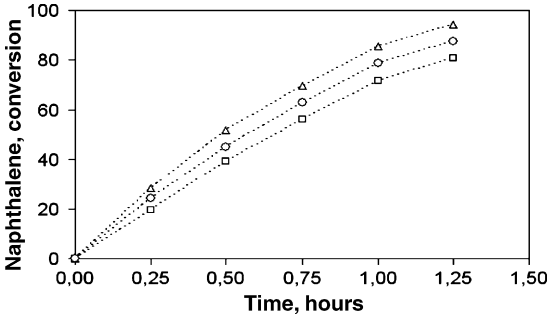

Fig. 3. Naphthalene conversion for NiMo/0ASA (□), NiMo/10ASA (△) and NiMo/25ASA (○) catalysts at 1200 psi and 598 K.

NiMo/10ASA reaches a conversion of nearly 94% compared with 88% and 81% displayed by NiMo/25ASA and NiMo/0ASA, respectively. It appears then that the incorporation of SiO_2 to the catalyst increases significantly the hydrogenation functionality of the catalyst. It is worth mentioning that the activity order of the catalysts is similar to that for the HDS of 4,6-DMDBT, for which the hydrogenation conversion route is important.

3.1.3. Carbazole hydrodenitrogenation

The conversion of carbazole after 5 h reaction time is 72% for NiMo/0ASA and NiMo/10ASA compared to 66% displayed by NiMo/25ASA (Fig. 4). These results indicate that for this reaction the incorporation of SiO_2 by the pH-swing method does not increase the HDN activity. Nevertheless, NiMo/10ASA seems to be the best choice due to its increased hydrogenation activity.

3.2. Kinetic study

To enquire more on the properties of each catalyst and the behaviour of each reaction type, a simplified kinetic study for each reaction (HDS of 4,6-DMDBT, HYD of naphthalene and HDN of carbazole) was carried out using Langmuir–Hinshelwood (L–H) type equations. Since hydrogen is in excess, its concentration remains almost constant throughout the reaction and therefore a pseudo-zero order was considered in the model. In addition, for the analysis, all the reactions were considered irreversible. Taking into account these restrictions; the following L–H equation was established:

$$-\frac{dC_i}{dt} = \frac{kC_i}{(1 + K_A C_i)^n}$$

where k represents the reaction rate constant; K_A stands for the adsorption constant; C_i is the concentration of the reactant component (4,6-DMDBT, naphthalene or carbazole) and n indicate the number of similar active sites involved in the reaction mechanism. Table 1 presents the estimated kinetic parameters for the L–H mechanisms that presented the best fit.

For the HDS of 4,6-DMDBT, an L–H type equation with two active sites presented the best correlation. Previously, Vrinat and Mourgues [22] reported a similar L–H equation type for the hydrodesulfurization of dibenzothiophene in presence of the H_2S formed in the reaction. In our case, the value of the reaction rate constant (k_{46}) increases when SiO_2 is present in the catalyst. For the different catalysts the values of k_{46} follow the order NiMo/10ASA > NiMo/25ASA > NiMo/0ASA, corroborating the higher activity of the NiMo/10ASA catalyst. On the other hand, the values of the K_{A46} adsorption constants for all the catalysts are similar (~112 L/mol), indicating that the composition of the Al–Si support does not affect the adsorption strength of the reactant on the active sites.

Table 1
Reaction rate and adsorption constants for 4,6-DMDBT HDS, naphthalene HYD and carbazole HDN

Catalyst	k (h^{-1})	K_A (L/mol)	R^2	L–H equation
4,6-DMDBT hydrodesulfurization				
NiMo/0ASA	3.28	107.06	0.9940	$-\frac{dC_{46}}{dt} = \frac{kC_{46}}{(1+K_A C_{46})^2}$
NiMo/10ASA	4.04	114.09	0.9950	
NiMo/25ASA	3.61	112.46	0.9941	
Naphthalene hydrogenation				
NiMo/0ASA	4.48	23.00	0.9928	$-\frac{dC_N}{dt} = \frac{kC_N}{1+K_A C_N}$
NiMo/10ASA	8.21	39.36	0.9855	
NiMo/25ASA	5.51	26.45	0.9093	
Carbazole hydrodenitrogenation				
NiMo/0ASA	0.42	223.07	0.9935	$-\frac{dC_C}{dt} = \frac{kC_C}{1+K_A C_C}$
NiMo/10ASA	0.49	284.99	0.9945	
NiMo/25ASA	0.43	269.57	0.9969	

For the HYD of naphthalene and HDN of carbazole, an L–H type equation with a single active site presented the best fit. In agreement with the kinetic study of 4,6-DMDBT, the value of the reaction rate constant for naphthalene (k_N) and carbazole (k_C) follow the same order (NiMo/10ASA > NiMo/25ASA > NiMo/0ASA). The k values for each reaction versus the SiO_2 content are displayed in Fig. 5. It is observed that regardless of the SiO_2 content the kinetic coefficients present the order: $k_N > k_{46} > k_C$.

The values of the adsorption constants show that naphthalene presents the lower interaction with the surface, indicating a weaker adsorption of this molecule (K_{AN}~30 L/mol). On the other hand, carbazole present a strong adsorption (K_{AC}~260 L/

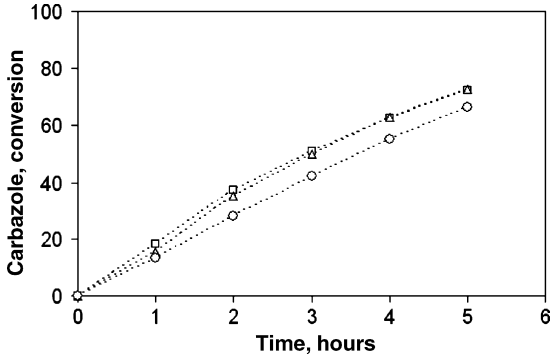

Fig. 4. Carbazole conversion for NiMo/0ASA (□), NiMo/10ASA (△) and NiMo/25ASA (○) catalysts at 1200 psi and 598 K.

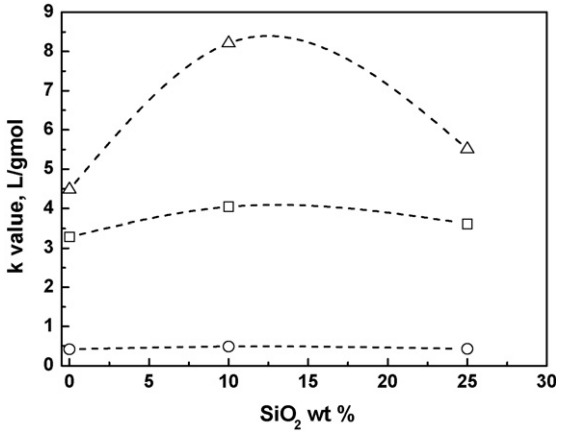

Fig. 5. Kinetic rate constant vs. SiO_2 wt% in the support for naphthalene (△), 4,6-DMDBT (□) and carbazole (○).

Table 2
Textural properties of supports and catalysts

Catalyst	BET surface area (m^2/g)		Pore volume (cm^3/g)		Average pore diameter (Å)	
	Support	Catalyst	Support	Catalyst	Support	Catalyst
NiMo/0 ASA	289	275	0.77	0.69	101	86
NiMo/10 ASA	381	308	0.95	0.77	100	81
NiMo/25 ASA	391	297	1.01	0.78	96	74

mol) over the active surface. So, carbazole is strongly adsorbed on the catalytic surface with respect to other reactants. As a consequence, carbazole poisons the active sites of the catalyst and inhibit the transformation of the other reactants. These results are in agreement with Koltai et al. [23] and Laredo et al. [24].

3.3. Characterization

3.3.1. Nitrogen physisorption

Table 2 shows the textural properties of supports and catalysts. The results indicate that the pH-swing method allows synthesizing catalysts with mesoporous structure. Fig. 6 presents the pore size distribution of the catalysts with different silica content. The curves show a monomodal distribution with a slight decrease in the average pore diameter when silica is added to support. Nevertheless, in the final catalysts the addition of silica to the support causes an increase in the pores of around 250 Å. Also, an increase in the surface area and pore volume near to 30% compared to 0ASA was observed. The impregnation of the NiMo phase causes a decrease of the surface area, pore volume and average pore diameter near to 20% for all samples with NiMo/10ASA presenting the highest surface area.

3.3.2. Surface coverage

The surface electric charge of the supports was measured by means of electrophoresis, obtaining the zero point charge or isoelectric point (not shown). Using the model proposed by Gil-Llambias et al. [25] the apparent surface coverage (ASC) of alumina by silica was determined. In this case, alumina is considered as the support and silica as the supported phase. The results show a nonlineal tendency between the apparent surface coverage and the amount of silica added to the support (see Fig. 7). Thus, we can assume that not all the silica incorporated by the pH-swing method is present on the surface of the Si–Al final support and that a significant part is contained in the bulk of the support.

3.3.3. FTIR hydroxyl region

To analyze the effect of silica incorporation on the structure of the support surface, the hydroxyl region of the FTIR spectra for all catalysts was analyzed. Fig. 8 shows the IR spectra of supports in the stretching O–H vibration region. The IR spectrum of pure alumina (0ASA) presents the characteristic bands of Al_2O_3 hydroxyl groups at 3790, 3775, 3730 and 3680 cm^{-1} [26–28]. According to Knözinger and Ratnasamy [28], the most basic hydroxyl groups bonded to aluminum in tetrahedral coordination give rise to an IR band at 3775 cm^{-1}. For the alumina support, this band is well evident. When silica is incorporated to alumina (10ASA), some changes in the band intensity are observed. The band corresponding to the most basic hydroxyl groups (3775 cm^{-1}) almost disappear. At the same time, a broad band with maxima at ~3740 cm^{-1} appears and develops into a more pronounced one for silica loadings of 25 and 50 wt%. This band is assigned to free silanol groups [29,30], indicating that at loadings higher than 10 wt% of SiO_2, the support surface is mostly silica. Therefore, one of the results of silica addition is the extinction of the basic hydroxyl groups (3775 cm^{-1}). In the past, the presence of these hydroxyl groups was related to the presence of inactive Mo phases [31,32], due to the strong interaction of these OH groups with the supported oxide phase. When these OH groups are eliminated, a decrease in the interaction of Mo oxide phase–support is expected.

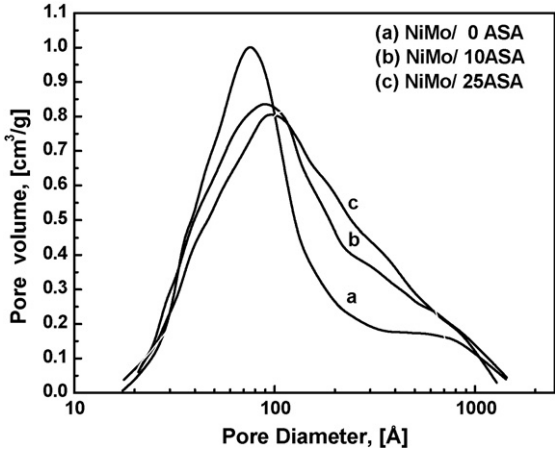

Fig. 6. Pore size distribution of NiMo/*X*ASA catalysts.

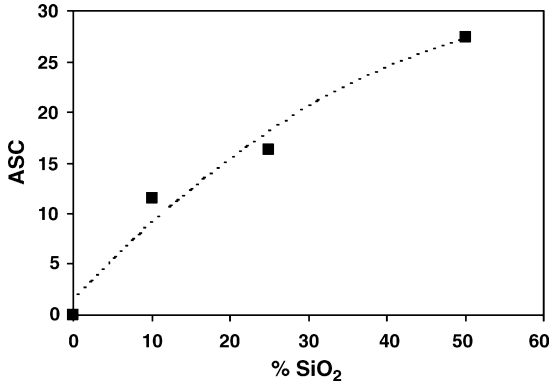

Fig. 7. Percent surface coverage (ASC) vs. silica content in the support.

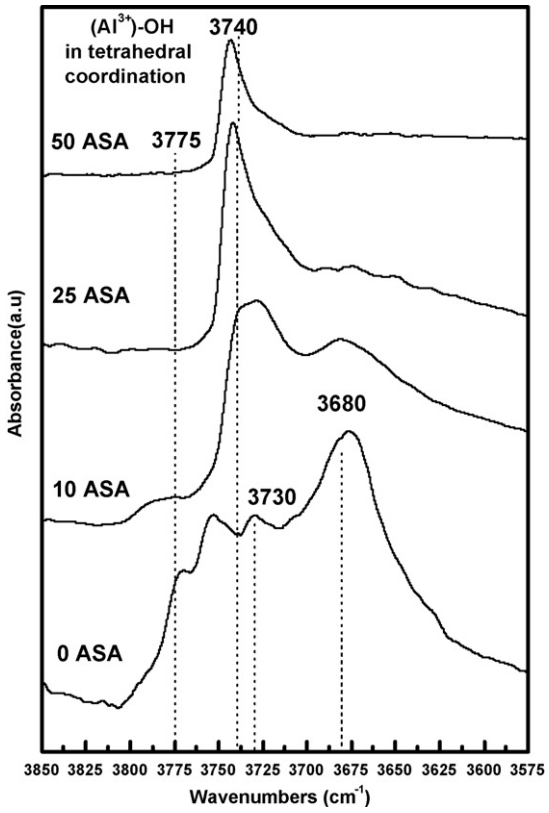

Fig. 8. FTIR spectra of supports in the hydroxyl region, after outgassing at 773 K for 1 h.

3.3.4. High-resolution transmission electron microscopy

To analyze the dispersion of the MoS_2 crystallites on the surface of the different catalysts HRTEM micrographs were obtained. Fig. 9 shows micrographs of the sulfided NiMo/*X*ASA catalysts. For NiMo/0ASA, the presence of homogeneously dispersed MoS_2 crystallites with mostly one layer is observed. In contrast, NiMo/10ASA and NiMo/25ASA catalysts show highly stacked MoS_2 crystallites.

Statistical analysis of the length and stacking of the crystallites (see Fig. 10) shows that the length distribution of MoS_2 crystallites changes when silica is present in the catalyst (NiMo/10ASA and NiMo/25ASA); an increase in the average crystallite length is observed. Similar results are observed in the stacking of the MoS_2 crystallites. NiMo/10ASA and NiMo/25ASA catalysts present an average number of layers of 2.3 compared to 1.6 displayed by NiMo/0ASA. The higher stacking of the MoS_2 crystallites seems to be the result of the lower interaction between the active phase and the support (SiO_2–Al_2O_3). It is expected that the higher stacking will favor the hydrogenation of aromatic rings, which interact during reaction with more than one coordinatively unsaturated Mo site [33].

3.3.5. FTIR-CO adsorption

CO adsorption on sulfided catalysts renders information about support surface and supported sulfided species. To inquire about surface species present on the sulfided NiMo catalysts, CO adsorption was performed. Fig. 11 shows the IR

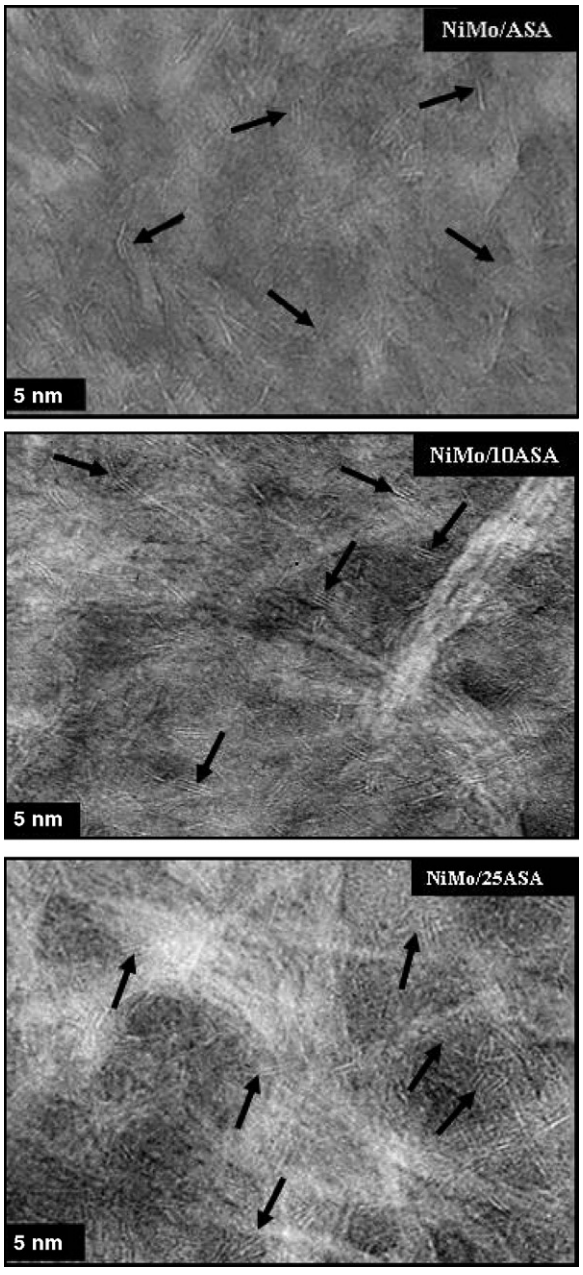

Fig. 9. HRTEM micrographs of sulfided NiMo/*X*ASA catalysts.

spectra of adsorbed CO at low temperature (100 K). For sulfided $NiMo/Al_2O_3$ catalysts, Travert et al. [34,35] reported the presence of six bands after CO adsorption at ~2190, 2156, 2120, 2110, 2085 and 2060–2045 cm^{-1}. The bands at 2190 and 2156 cm^{-1} have been assigned to CO adsorbed on coordinative unsaturated sites of Al^{3+} (Lewis sites) and CO in hydrogen bonding with support hydroxyl groups, respectively. The bands at 2120, 2110, 2085 and 2060–2045 cm^{-1} are associated to CO adsorbed on CUS sites of different sulfided Ni and Mo phases [34–37] After CO adsorption on NiMo 0ASA three well defined bands appear at 2190, 2155 and ~2125 cm^{-1}, and shoulders at 2110, 2080, and 2050 cm^{-1}. These bands have been well characterized by Travert et al. [34]. Silica incorporation (10 and 25 wt%) to alumina causes some changes in the intensity and frequency of IR bands: (1) As was expected, a gradual decrease

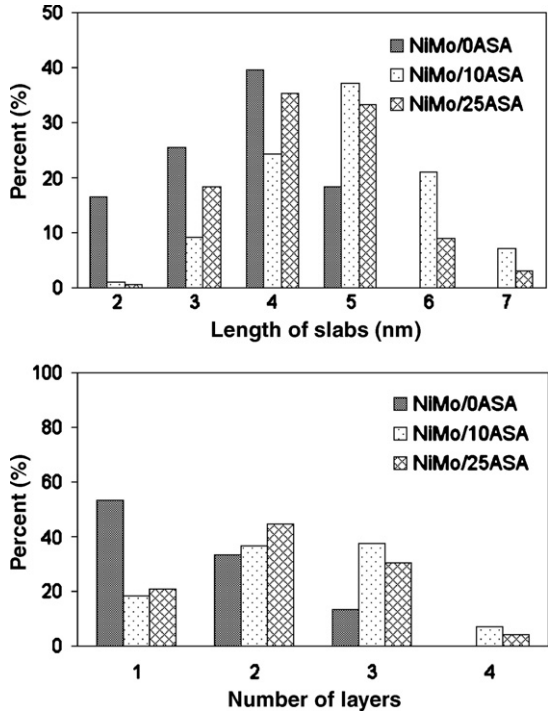

Fig. 10. MoS_2 crystallite size distribution for sulfided NiMo/*X*ASA catalysts.

in the band intensity related to Lewis acidic sites (CUS-Al^{3+}, 2190 cm^{-1}), being less intense at the highest silica loading. Fig. 11 also shows an increment in the amount of coordinatively unsaturated sites (CUS), which are related to active sites (band at ~2125 cm^{-1}), with the silica content. (2) The position of the band region associated to sulfided phases is shifted upward, from 2040–1125 to 2050–2150 cm^{-1}. The position of the CO bands is affected by the backdonation of d-electrons from the adsorption center (sulfided phase). When this backdonation is low, the IR band position is shifted to higher frequencies, as observed in Fig. 11 when silica was added to the catalysts. This behaviour could be explained by a decrease in the electronic density of the sulfided phases caused by an increase in the acidic strength of the support surface when silica is added.

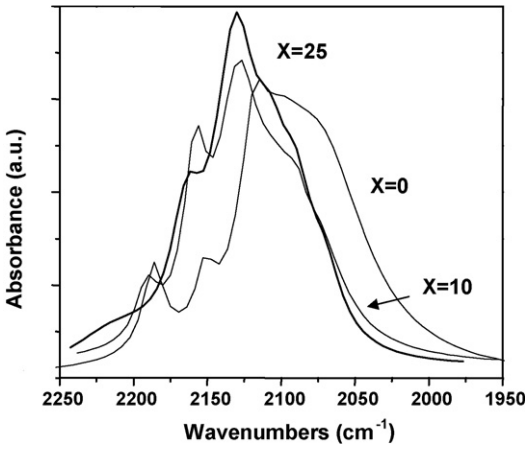

Fig. 11. FTIR spectra after CO adsorption on NiMo/*X*ASA at 1 Torr equilibrium.

Summarizing, the above results indicate that the activity of NiMo catalysts supported over SiO_2–Al_2O_3 for the HDS, HYD and HDN reactions depend on the silica/alumina ratio on the support. For 4,6-DMDBT HDS, when 10 and 25 wt% SiO_2 was incorporated on the support, the value of the reaction rate constant increased 1.23 and 1.1 times with respect to the silica-free catalyst (NiMo/0ASA). Similar results were observed in the naphthalene hydrogenation. For carbazole HDN, the incorporation of silica to the support does not cause an important effect and therefore the catalysts present similar activity. The changes in catalytic activity with the addition of silica may be associated in part to the elimination of the most basic hydroxyl groups bonded to aluminum in tetrahedral coordination. This elimination of the most reactive hydroxyl groups in alumina causes a decrease in the Mo oxide phase–support interaction, leading to a good sulfidation of the NiMo phase and higher stacking of MoS_2 crystallites. Highly stacked MoS_2 crystallites provide a better probability of formation of the multiple sulfur vacancies needed for the hydrogenation reaction. In line with this, the hydrogenation activity increases with the silica content. The analysis of CO adsorption on the sulfided catalyst corroborated an increase in the amount of coordinatively unsaturated sites (CUS) with the incorporation of silica to the catalyst. The best silica/alumina ratio on the support was obtained with NiMo/10ASA catalyst (10 wt% SiO_2).

4. Conclusions

The pH-swing method allowed the synthesis of a SiO_2–Al_2O_3 support with silica contents of 10 and 25 wt% SiO_2. NiMo/10ASA catalyst showed the highest activity for HYD of naphthalene, HDS of 4,6-DMDBT and HDN of carbazole. The increase in activity when silica is present in the support is in part related to the elimination of the support OH groups bonded to Al^{3+} in tetrahedral coordination. The surface modification of alumina with silica generates a lower interaction between the Mo oxide phase and the support leading to a good sulfidation of the active NiMo phase and high stacking of the MoS_2 crystallites. These changes in the active phase properties induce an increase in the number of active sites, which can be related to the CUS titrated by CO adsorption.

Acknowledgments

The authors are grateful for financial support through UNAM DGAPA-PAPIIT IN-101406 project, CONACyT Project 49479 and CONACyT-CSIC program. To Ivan Puente Lee for HRTEM work. PTM, FSM, and CFV thank CONACyT (México) for their Ph.D. fellowships.

References

[1] P.T. Vasudevan, J.L.G. Fierro, Catal. Rev. Sci. Eng. 38 (1996) 161.
[2] H. Topsøe, B.S. Clausen, F.E. Massoth, in: J.R. Anderson, M. Boudart (Eds.), Hydrotreating Catalysis, Science and Technology, vol. 11, Springer, Berlin, 1996 (chapter 1–3).

[3] M.V. Landau, D. Berger, M. Herskowitz, J. Catal. 159 (1996) 236.
[4] K.G. Knudsen, B.H. Cooper, H. Topsøe, Appl. Catal. A 189 (1999) 205.
[5] T. Kabe, Y. Aoyama, D. Wang, A. Ishihara, W. Qian, M. Hosoya, Q. Zhang, Appl. Catal. A 209 (2001) 237.
[6] G. Pérot, Catal. Today 86 (2003) 111.
[7] K. Naoyuki, Ch. Ki-Hyouk, Y. Korai, I. Mochida, K. Nakano, Catal. Today 86 (2003) 73–85.
[8] P. Michaud, J.L. Lemberton, G. Pérot, Appl. Catal. A 169 (1998) 343.
[9] F. Bataille, J.L. Lemberton, P. Michaud, G. Pérot, M. Vrinat, M. Lemaire, E. Schulz, M. Breysse, S. Kasztelan, J. Catal. 191 (2000) 409.
[10] H. Kim, J.J. Lee, S.H. Moon, Appl. Catal. B 44 (2003) 287.
[11] M. Egorova, R. Prins, J. Catal. 225 (2004) 417.
[12] T. Isoda, S. Nagao, X. Ma, Y. Korai, I. Mochida, Appl. Catal. A 150 (1997) 1.
[13] E. Lecrenay, K. Sakanishi, I. Mochida, T. Suzuka, Appl. Catal. A 175 (1998) 237.
[14] M. Egorova, R. Prins, J. Catal. 224 (2004) 278.
[15] M. Fernandez-Garcia, E.G. Rebollo, A.G. Ruiz, J.C. Conesa, J. Soria, J. Catal. 172 (1997) 146.
[16] W.R.A.M. Robinson, J.A.R. wan Veen, V.H.J. de Beer, R.A. van Santen, Fuel Process Technol. 61 (1999) 89.
[17] B. Pawelec, R.M. Navarro, J.M. Campos-Martin, A. Lopez Agudo, P.T. Vasudevan, J.L.G. Fierro, Catal. Today 86 (2003) 73.
[18] R.K. Denni, Patent 4,721,696 (January 26, 1988).
[19] T. Ono, Y. Ohguchi, O. Togari, Preparation of Catalysts III, Elsevier Science Publisher, The Netherlands, 1983.
[20] R. Snell, Appl. Catal. 11 (1984) 189–347.
[21] C. Fernández-Vargas, J. Ramírez-Solís, A. Gutiérrez-Alejandre, J. Sánchez-Minero, P. Torres-Mancera, Characterization of NiMo/SiO_2–Al_2O_3 catalysts prepared by the pH-swing method, in: Proceedings of the XX Iberoamerican Symposium on Catalysis, September 17–22, 2006.
[22] M.L. Vrinat, L. Mourgues, J. Chim. Phys. 79 (1982) 45.
[23] T. Koltai, M. Macaud, A. Guevara, E. Schulz, M. Lemaire, R. Bacaud, M. Vrinat, Appl. Catal. A 231 (2002) 253.
[24] G.C. Laredo, A. Montesinos, J.A. De los Reyes, Appl. Catal. A 265 (2004) 171.
[25] F.J. Gil-Llambias, A.M. Escudey-Castro, A. Lopez-Agudo, J. Chem. Soc., Chem. Commun. 478 (1982).
[26] N. Katada, T. Fujii, K. Iwata, Y. Hibino, M. Niwa, J. Catal. 186 (1999) 478.
[27] M. Digne, P. Sautet, P. Raybaud, P. Euzen, H. Toulhoat, J. Catal. 211 (2002) 1.
[28] H. Knözinger, P. Ratnasamy, Catal. Rev. 17 (2005) 31.
[29] D. Bianchini, J.H. Zimnoch dos Santos, T. Uozumi, Tsuneji Sano, J. Mol. Catal. A 185 (2002) 223.
[30] S. Pallavi, V.A. Ramaswamy, Karoly Lazar, Veda Ramaswamy, Appl. Catal. A 273 (2004) 239.
[31] R. Cuevas, J. Ramírez, G. Busca, J. Fluorine Chem. 122 (2003) 151.
[32] M. Sun, D. Nicosia, R. Prins, Catal. Today 86 (2003) 173.
[33] L. Qu, W. Zhang, P.J. Kooyman, R. Prins, J. Catal. 215 (2003) 7–13.
[34] A. Travert, C. Dujardin, F. Maugé, E. Veilly, S. Cristol, J.F. Paul, E. Payen, J. Phys. Chem. B 110 (2006) 1261–1270.
[35] A. Travert, C. Dujardin, F. Maugé, S. Cristol, J.F. Paul, E. Payen, D. Bougeard, Catal. Today 70 (2001) 255–269.
[36] K. Gòra-Marek, M. Derewìnski, P. Sarv, J. Datka, Catal. Today 101 (2005) 131–138.
[37] J. Choi, F. Maugé, C. Pichon, J. Olivier-Fourcade, J. Jumas, C. Petit-Clair, D. Uzio, Appl. Catal. A: Gen. 267 (2004) 203–216.